GLOBAL CARBON CYCLE

The reinvigoration of the Southern Ocean carbon sink

Peter Landschützer,[1]* Nicolas Gruber,[1,2] F. Alexander Haumann,[1,2] Christian Rödenbeck,[3] Dorothee C. E. Bakker,[4] Steven van Heuven,[5]† Mario Hoppema,[5] Nicolas Metzl,[6] Colm Sweeney,[7,8] Taro Takahashi,[9] Bronte Tilbrook,[10] Rik Wanninkhof[11]

Several studies have suggested that the carbon sink in the Southern Ocean—the ocean's strongest region for the uptake of anthropogenic CO_2—has weakened in recent decades. We demonstrated, on the basis of multidecadal analyses of surface ocean CO_2 observations, that this weakening trend stopped around 2002, and by 2012 the Southern Ocean had regained its expected strength based on the growth of atmospheric CO_2. All three Southern Ocean sectors have contributed to this reinvigoration of the carbon sink, yet differences in the processes between sectors exist, related to a tendency toward a zonally more asymmetric atmospheric circulation. The large decadal variations in the Southern Ocean carbon sink suggest a rather dynamic ocean carbon cycle that varies more in time than previously recognized.

Simulations with ocean biogeochemical models have suggested a stagnation or even a reduction of the Southern Ocean carbon sink from the 1980s to the early 2000s (*1*–*3*), a result that has been supported by inversion studies (*1*) based on atmospheric CO_2 data. Such a stagnation has wide-reaching implications for climate, because the Southern Ocean south of 35°S accounts for about 40% of the global oceanic uptake of anthropogenic CO_2 (*4*–*6*), thereby removing a disproportionally large share of anthropogenic CO_2 from the atmosphere. The trend toward a saturation of the Southern Ocean carbon sink has been attributed mainly to the intensification and poleward shift of the westerly winds associated with a trend toward a more positive state of the Southern Annular Mode (*1*, *2*). The resulting enhanced upwelling of deep waters with high concentrations of dissolved inorganic carbon (DIC) drove an anomalously strong flux of natural CO_2 out of the surface ocean, counteracting the increase in the oceanic uptake of anthropogenic CO_2 (*2*).

Several studies based on observations of the surface partial pressure of CO_2 (pCO_2) (*7*–*9*) corroborated these model-based trends in the Southern Ocean carbon sink, but all of them used the observations without any interpolation. Given the sparsity and spatial heterogeneity of these surface ocean observations (*8*), the conclusions drawn in these studies regarding the trends turn out to be rather sensitive to the chosen method of trend calculation (*9*) and the beginning and end year of analysis (*10*). Nevertheless, these studies tended to support a weakening sink trend up to the mid-2000s. One of these studies (*9*) also pointed out that the trend may have reversed in recent years, a finding corroborated by the analysis of pCO_2 observations along a single meridional transect south of Tasmania (*11*).

To address the sparse data coverage, we used a neural network technique (*12*) to interpolate the pCO_2 observations in time and space. We then evaluated the results using (i) a complementary pCO_2 observation–based product based on the interpolation by a data-driven mixed-layer scheme (*13*) and (ii) an atmospheric CO_2 inverse estimate (*14*). Both surface ocean–based methods were extended for this study to produce multidecadal distributions of the surface ocean pCO_2 field (*15*–*17*). The air-sea CO_2 flux variations were then computed with the use of a standard bulk parameterization (supplementary text 1.4). Although each of these estimates faces limits due to the available information, their combination allows us to gain confidence in the inferred features.

The two surface ocean data–based air-sea CO_2 flux products confirm that the Southern Ocean carbon sink (south of 35°S) weakened through much of the 1990s, in agreement with the model-based studies and the atmospheric inversions (*1*, *2*), but they reveal that it has strengthened substantially since about 2002, increasing by more than ~0.6 Pg of C $year^{-1}$ (Fig. 1) to a vigorous uptake of ~1.2 Pg of C $year^{-1}$ in 2011. This increase has returned the Southern Ocean sink to levels expected from the increase in atmospheric CO_2 (*5*), computed from an ocean biogeochemistry model forced with just the increase in atmospheric CO_2 (*18*). The increase in the Southern Ocean carbon uptake since 2002 is responsible for roughly half of the global trend in the ocean carbon sink over this period (*15*), highlighting the importance of the Southern Ocean in moderating the growth of atmospheric CO_2.

Both surface ocean observation–based methods rely on the to-date largest sea surface pCO_2 observation database [Surface Ocean CO_2 Atlas (SOCAT) version 2] (*19*), which contains more than 2.6 million observations in the Southern Ocean south of 35°S. The neural network technique (*12*, *15*) interpolates these observations

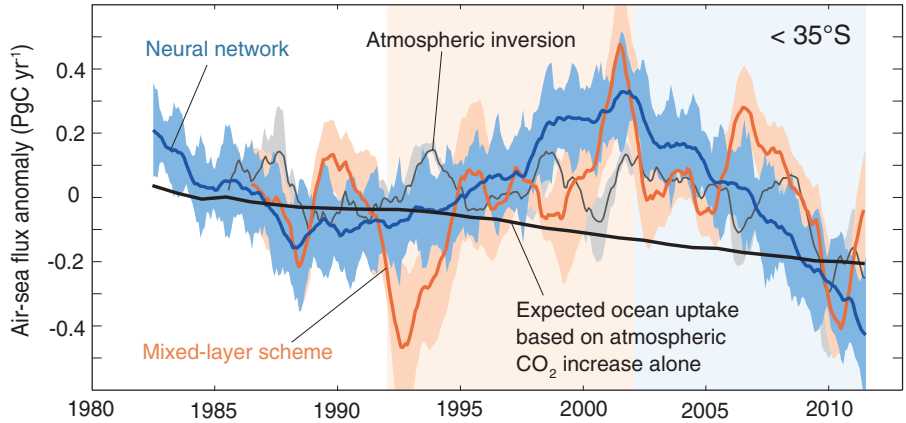

Fig. 1. Evolution of the Southern Ocean carbon sink anomaly south of 35°S. The lines show the integrated air-sea CO_2 flux derived from two complementary surface ocean pCO_2 interpolation methods [a two-step neural network technique (*15*) and a mixed-layer scheme (*17*)] as well as the integrated flux from an atmospheric inversion based on measurements of atmospheric CO_2 (*14*). These estimates are compared with the expected uptake based on the growth of atmospheric CO_2 alone, based on a simulation with the ocean component of the Community Climate System Model (CCSM3) (*18*). All data are plotted as anomalies by subtracting the 1980s mean flux from each method. Negative values indicate anomalous uptake by the ocean.

[1]Environmental Physics, Institute of Biogeochemistry and Pollutant Dynamics, ETH Zürich, Zürich, Switzerland. [2]Center for Climate Systems Modeling, C2SM, ETH Zürich, Zürich, Switzerland. [3]Max Planck Institute for Biogeochemistry, Jena, Germany. [4]Centre for Ocean and Atmospheric Sciences, School of Environmental Sciences, University of East Anglia, Norwich, UK. [5]Alfred Wegener Institute Helmholtz Centre for Polar and Marine Research, Bremerhaven, Germany. [6]Sorbonne Universités (UPMC, Univ Paris 06)-CNRS-IRD-MNHN, LOCEAN/IPSL Laboratory, 4 place Jussieu, F-75005 Paris, France. [7]Cooperative Institute for Research in Environmental Science, University of Colorado, Boulder, CO 80309, USA. [8]National Oceanic and Atmospheric Administration (NOAA) Earth System Research Laboratory, Boulder, CO, USA. [9]Lamont-Doherty Earth Observatory of Columbia University, Palisades, NY, USA. [10]Commonwealth Scientific and Industrial Research Organisation and Antarctic Climate and Ecosystems Co-operative Research Centre, Hobart, Australia. [11]Atlantic Oceanographic and Meteorological Laboratory of NOAA, Miami, FL, USA.
***Corresponding author. E-mail: peter.landschuetzer@usys.ethz.ch** †Present address: Department of Marine Geology and Chemical Oceanography, Royal Netherlands Institute for Sea Research (NIOZ), Texel, Netherlands.

to a 1° × 1° global grid at a monthly resolution for the period from 1982 through 2011, resulting in a multidecadal reconstruction of the global ocean carbon sink. The method relies on nonlinear but robust relations between the limited pCO_2 observations and the properties that are measured more frequently, such as sea surface temperature, sea surface salinity, satellite measurements of chlorophyll a, and mixed-layer depth (supplementary text 1.2). The mixed-layer scheme (*13*, *17*) (version oc_v1.2), in contrast, does not regress pCO_2 variations to physical, chemical, or biological driver data but directly assimilates the available pCO_2 observations into a mass budget of the mixed layer at a resolution of 4° × 5° in space and daily in time. This method also uses several ancillary observations to parameterize the air-sea CO_2 exchange, solubility, and carbon chemistry but does not use them to interpolate the pCO_2 to regions without observations. Instead, it interpolates the pCO_2 data directly.

Extensive validation of the neural network–based estimate using independent observations reveals that the method is able to map the sparse pCO_2 data with little bias (with mean differences between SOCAT observations and neural network estimates of generally less than 2 µatm; table S1) in space and time. Both methods agree well regarding the sign and the magnitude of the decadal trends within the two decades from 1992 through 2001 and 2002 through 2011 (Fig. 1 and table S2), when the majority of surface ocean pCO_2 observations were made (fig. S3).

However, given the methodological differences in the data treatment in data-sparse regions (interpolation versus regression), there is less agreement regarding higher-frequency variability such as the year-to-year variations in the sink strength. This lower agreement is a result of the weaker signal-to-noise ratio of the pCO_2 data in the interannual frequency band. Under such conditions, the direct interpolation scheme of the mixed-layer method tends to extrapolate high-frequency noise present in the observations to the data-sparse regions, probably generating overly strong variations there. In contrast, the neural network scheme suppresses the high-frequency noise by being constrained by the ancillary observations, resulting in a possible underestimation of the year-to-year variability in the data-sparse regions. In contrast, the relatively strong pCO_2 signals that underlie the decadal changes in the Southern Ocean are distinctly captured by the two methods, resulting in very similar decadal trends.

The changes in the Southern Ocean carbon sink are almost entirely driven by changes in the air-sea difference of pCO_2; i.e., $\Delta pCO_2 = pCO_2^{sea} - pCO_2^{atm}$ (pCO_2^{atm} = atmospheric pCO_2), because the direct effect of changes in the wind and temperature on the gas transfer coefficient is small (fig. S8). The spatial pattern of the trends in ΔpCO_2 from the neural network method reveals for both decades a very uniform trend pattern across the entire Southern Ocean, with the strongest ΔpCO_2 trends at high latitudes (Fig. 2, A and B). The spatial trends for the mixed-layer scheme are similar, although at coarser resolution and with somewhat more zonal variations, part of which may be spurious because of missing data constraints there, reflecting the more variance-producing nature of this method in data-sparse regions (fig. S6). From 1992 through 2001, the trend in ΔpCO_2 was strongly positive, driven by the surface ocean pCO_2 increasing at nearly twice the rate of pCO_2^{atm} around Antarctica. In contrast, from 2002 onward, the growth of surface ocean pCO_2 nearly stalled, strongly increasing the degree of surface ocean undersaturation, which ultimately drove the increasing uptake of atmospheric CO_2.

We tested the robustness of this result on the basis that such strong decadal changes in the CO_2 uptake across most of the Southern Ocean should leave an imprint on atmospheric CO_2, taking advantage of the lack of land regions with substantial CO_2 fluxes south of 35°S. Specifically, we used an atmospheric inversion method (*14*) to infer the air-sea CO_2 fluxes that are optimally consistent with the atmospheric CO_2 data, while taking into consideration atmospheric transport and mixing. The setup of the employed version s85_v3.7 uses the atmospheric winds from the ERA-Interim reanalysis (*20*). The evolution of the Southern Ocean carbon sink from this inversion of atmospheric CO_2 data also supports our postulated larger–than-expected increase in the strength of the Southern Ocean carbon

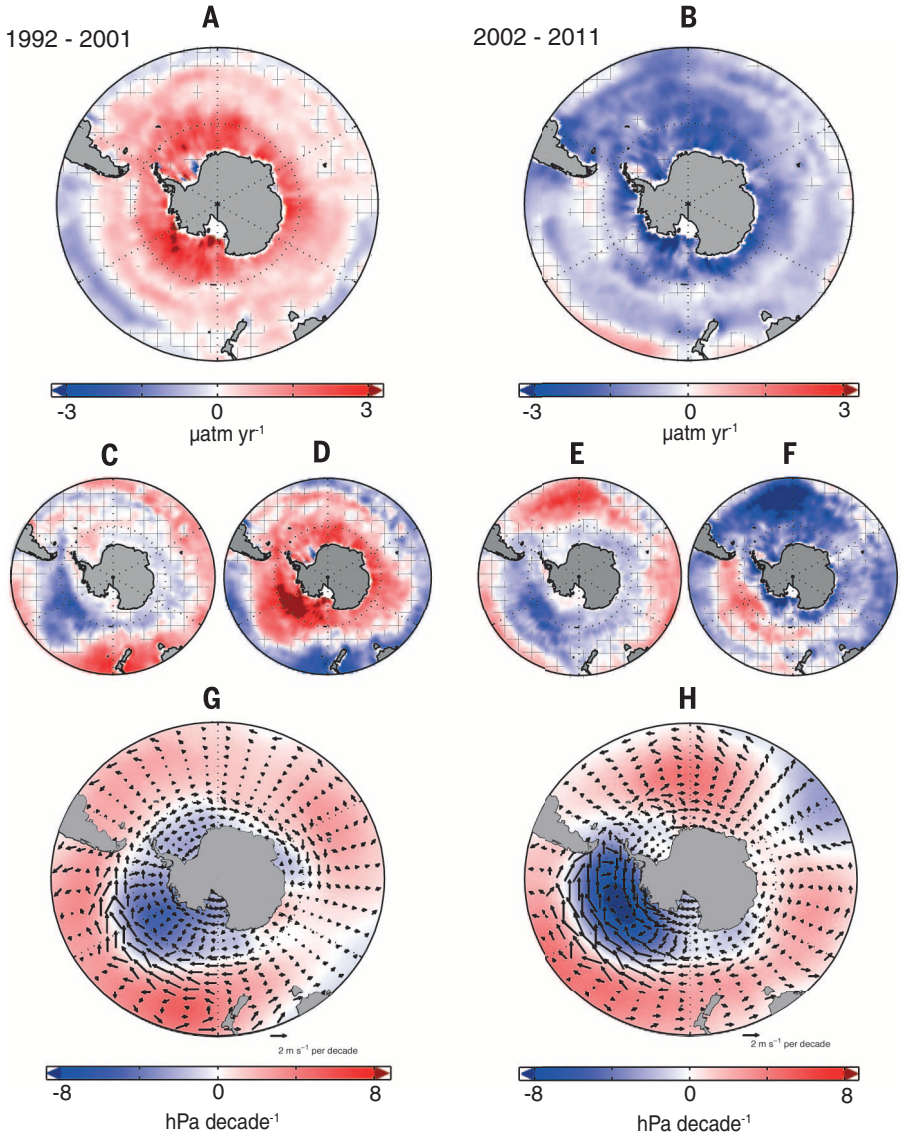

Fig. 2. Trends in ΔpCO_2 based on the neural network output and its two components for the two analysis decades: 1992 through 2001 and 2002 through 2011. (**A**) Linear trend in ΔpCO_2 for the 1990s. (**B**) As (A) but for the 2000s. Linear trend in (**C**) thermal pCO_2 and (**D**) nonthermal ΔpCO_2 for the 1990s. (**E**) and (**F**), as (C) and (D) but for the 2000s. Positive (red) ΔpCO_2 trends indicate a faster increase of pCO_2 in the surface ocean than in the atmosphere (i.e., a decreasing sink) and vice versa for positive (blue) trends. Hatched areas indicate where the linear trends are outside the 5% significance level ($P \geq 0.05$). (**G**) and (**H**) illustrate decadal trends of sea level pressure (shading) and 10-m wind (vectors) from 1992 through 2001 (G) and 2002 through 2011 (H) based on data from the ERA-Interim reanalysis (*20*).

sink within the past decade (Fig. 1), even though it shows much less of a weakening during the 1990s. Thus, two complementary pCO_2 database estimates, as well as an atmospheric CO_2 inversion, confirm that the Southern Ocean carbon sink has experienced a significant strengthening since the early 2000s.

This reinvigoration after the early 2000s cannot be a simple reversal of the Southern Annular Mode–driven wind trend that has been suggested to cause the weakening of the Southern Ocean carbon sink over the past decades (*1*, *2*), because the ERA-Interim reanalysis winds (*20*) do not show such a signal (Fig. 2, G and H). Instead, the atmospheric circulation became more zonally asymmetric with a wavenumber two pattern, reminiscent of the lower-frequency pattern of variability of the Antarctic Circumpolar Wave (*21*). But how can this zonally asymmetric forcing result in a relatively zonally uniform response of the surface ocean pCO_2?

Insight into the drivers is gained by separating the ΔpCO_2 trend pattern into a component driven by changes in sea surface temperature [the thermal trend (Fig. 2, C and E)] and one driven by changes in the DIC and/or alkalinity [the nonthermal trend (Fig. 2, D and F)] (*22*). For both analysis periods, the trends in the thermal and nonthermal components are generally opposed for any given location, which is in line with previous studies (*22*–*24*). The thermal component shows a sink increase in both decades in the Pacific sector, where the advection of cold air from Antarctica and sea-ice changes led to a persistent surface cooling trend (*25*). In the lower latitudes of the Atlantic and Indian sectors, we find a reduced thermally driven uptake in the 2000s due to surface ocean warming, which is probably related to the more asymmetric atmospheric circulation that caused a reduced northward Ekman transport (fig. S11) of cold polar waters in these regions.

In the nonthermal component, we find more distinct differences between the two periods. Between 1992 and 2001, the nonthermal component increased the oceanic pCO_2 over most of the Southern Ocean (Fig. 2D), in particular in the high latitudes and in the Pacific sector. The estimated changes in Ekman pumping velocity [estimated from ERA-Interim winds (*20*), fig. S11] support the hypothesis that wind changes led to an increased surface divergence and an associated upwelling of DIC-rich waters into all sectors of the high-latitude Southern Ocean (*2*) in the first period. During the subsequent period, the nonthermal component primarily reduced the oceanic pCO_2 in the Atlantic and Indian sectors and over the Antarctic shelf (Fig. 2F). In contrast, this component continued to increase pCO_2 in most of the Pacific sector, although at a much weaker rate than in the 1990s. This much weaker DIC- and/or alkalinity-induced increase in pCO_2 in the Pacific sector could no longer compensate for the thermal trend, so that the negative trend in the total pCO_2 in this region for the period after 2001 is dominated by the thermal trend. In contrast, in the Atlantic and Indian sectors and over the Antarctic shelf, the negative nonthermal trend dominates the thermal changes. Thus, overall, the temperature-dominated pCO_2 trend in the Pacific sector and the DIC/alkalinity–driven trend in the other regions have worked in tandem to prevent pCO_2 from increasing across the entire Southern Ocean since the early 2000s. Over the same period, atmospheric CO_2 continued to rise strongly, resulting in a substantial increase in the undersaturation of the surface ocean with regard to atmospheric CO_2, hence driving a strong increase in the flux of CO_2 into the entire Southern Ocean.

We interpret this zonal asymmetry of thermally and DIC/alkalinity–driven changes to be primarily the result of an increased asymmetry in the Southern Hemisphere atmospheric circulation in the years since 2001 (Fig. 3). Specifically, the conditions became more cyclonically dominant in the Pacific sector, and more anti-cyclonically dominant in the Atlantic and parts of the Indian sector (Fig. 2H). As a result of the associated increase in the meridional wind components, more cold air was advected from the Antarctic continent over the Pacific sector, and more warm air was advected from subtropical latitudes over the Atlantic and part of the Indian sectors. Together with the changes in northward Ekman transport (fig. S11), this provides an explanation for the strengthened asymmetry in the sea surface temperature trends, which underlie the thermal trends in Fig. 2E.

A strengthening of the carbon sink in the Pacific sector, combined with the further intensification of the winds (Fig. 2H) during the 2000s, provide a paradox at first sight, because the increased upwelling in the Pacific sector should have increased the surface DIC content further. A possible explanation is that the recent stabilization of the surface waters (*26*) counteracted

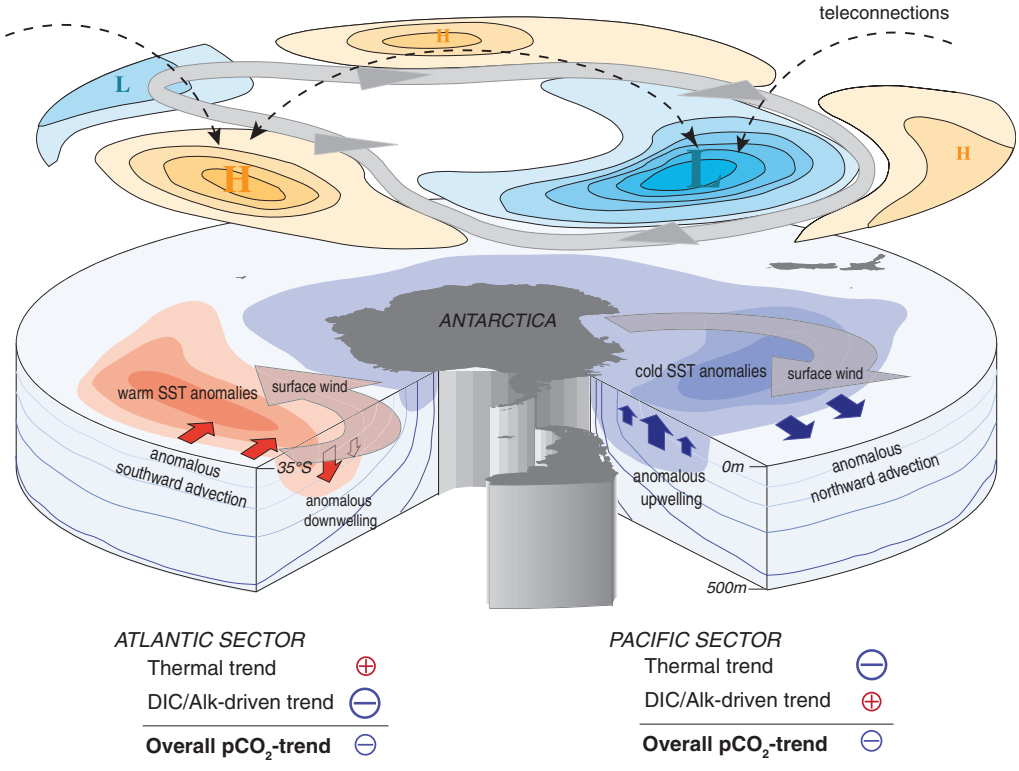

Fig. 3. Schematic of the processes governing the changes in the ΔpCO_2 trends in the Southern Ocean since 2001. The trend toward a zonally more asymmetric distribution of the atmospheric pressure systems in the past decade led to stronger meridional winds bringing either colder air (Pacific sector) or warmer air (Atlantic sector) to the open Southern Ocean, causing strong cooling of the sea surface in the Pacific sector and warming in the Atlantic sector. The changes in wind also affected the oceanic circulation pattern, with the net effect being an increase in the DIC/alkalinity–driven pCO_2 component in the Pacific sector and a decrease of this component in the Atlantic sector (i.e., opposing the effect of sea surface temperature on pCO_2). In the Pacific sector, the effect of the cooling trend on pCO_2 prevails, whereas in the Atlantic sector, the effect of circulation/mixing on DIC/alkalinity prevails, also causing a lowering trend in pCO_2. Thus, owing to the interaction between temperature and circulation changes, the zonally asymmetric forcing caused a zonally relatively symmetric response of the ocean carbon sink.

the wind-induced upwelling. In the Pacific sector and in coastal regions, strong surface freshening (*26*, *27*) might have caused most of this stabilization, whereas in the lower latitudes of the Atlantic and Indian sectors, warming stabilized the surface waters. The reduction in northward Ekman transport to the lower-latitude Atlantic and Indian sectors during the 2000s (fig. S11), which is probably the result of the zonally more asymmetric atmospheric circulation, also reduced the northward advection of high-latitude waters, lowering the DIC content and/or increasing the alkalinity at the surface.

The trend toward a zonally more asymmetric atmospheric circulation may be related to long-term variations of the tropical sea surface temperature; i.e., to the more prevalent La Niña conditions in the Pacific since the early 2000s (*28*) and the more positive phase of the Atlantic Multidecadal Oscillation over recent decades (*29*). Alternatively, it may be driven by a zonally asymmetric response of the Southern Hemisphere near-surface circulation to the anthropogenic forcing (*25*).

Our results indicate that Earth's most important sink for anthropogenic CO_2 (*5*, *6*) is more variable than previously suggested and that it responds quite sensitively to physical climate variability. This also suggests that should current climate trends reverse in the near future, the Southern Ocean might lose its recently regained uptake strength, leading to a faster accumulation of CO_2 in the atmosphere and consequently an acceleration of the rate of global warming.

REFERENCES AND NOTES

1. C. Le Quéré *et al.*, *Science* **316**, 1735–1738 (2007).
2. N. S. Lovenduski, N. Gruber, *Global Biochem. Cyc.* **22**, GB3016 (2008).
3. A. Lenton *et al.*, *Biogeosciences* **10**, 4037–4054 (2013).
4. C. L. Sabine *et al.*, *Science* **305**, 367–371 (2004).
5. S. E. Mikaloff Fletcher *et al.*, *Global Biogeochem. Cycles* **20**, GB2002 (2006).
6. T. L. Frölicher *et al.*, *J. Clim.* **28**, 862–886 (2015).
7. N. Metzl, *Deep Sea Res. Part II Top. Stud. Oceanogr.* **56**, 607–619 (2009).
8. T. Takahashi *et al.*, *Oceanography* **25**, 26–37 (2012).
9. A. R. Fay, G. A. McKinley, N. S. Lovenduski, *Geophys. Res. Lett.* **41**, 6833–6840 (2014).
10. N. S. Lovenduski, A. R. Fay, G. A. McKinley, *Global Biogeochem. Cyc.* **29**, 416–426 (2015).
11. L. Xue, L. Gao, W.-J. Cai, W. Yu, M. Wei, *Geophys. Res. Lett.* **42**, 3973–3979 (2015).
12. P. Landschützer *et al.*, *Biogeosciences* **10**, 7793–7815 (2013).
13. C. Rödenbeck *et al.*, *Ocean Science* **9**, 193 (2013).
14. C. Rödenbeck, S. Houweling, M. Gloor, M. Heimann, *Atmos. Chem. Phys.* **3**, 1919–1964 (2003).
15. P. Landschützer, N. Gruber, D. C. E. Bakker, U. Schuster, *Global Biogeochem. Cyc.* **28**, 927–949 (2014).
16. P. Landschützer, N. Gruber, D. C. E. Bakker, *A 30 Years Observation-Based Global Monthly Gridded Sea Surface pCO_2 Product from 1982 Through 2011* (Carbon Dioxide Information Analysis Center, Oak Ridge National Laboratory, U.S. Department of Energy, Oak Ridge, TN, 2015).
17. C. Rödenbeck *et al.*, *Biogeosciences* **11**, 4599–4613 (2014).
18. H. D. Graven, N. Gruber, R. Key, S. Khatiwala, X. Giraud, *J. Geophys. Res.* **117**, C10005 (2012).
19. D. C. E. Bakker *et al.*, *Earth System Sci. Data* **6**, 69–90 (2014).
20. D. P. Dee *et al.*, *Q. J. R. Meteorol. Soc.* **137**, 553–597 (2011).
21. A. F. Carril, A. Navarra, *Geophys. Res. Lett.* **28**, 4623–4626 (2001).
22. T. Takahashi *et al.*, *Deep Sea Res. Part II Top. Stud. Oceanogr.* **49**, 1601–1622 (2002).
23. N. Gruber *et al.*, *Global Biogeochem. Cycles* **23**, GB1005 (2009).
24. J. D. Majkut, J. L. Sarmiento, K. B. Rodgers, *Global Biogeochem. Cycles* **28**, 335–351 (2014).
25. F. A. Haumann, D. Notz, H. Schmidt, *Geophys. Res. Lett.* **41**, 8429–8437 (2014).
26. C. De Lavergne, J. B. Palter, E. D. Galbraith, R. Bernardello, I. Marinov, *Nat. Clim. Change* **4**, 278–282 (2014).
27. S. S. Jacobs, C. F. Giulivi, *J. Clim.* **23**, 4508–4524 (2010).
28. Q. Ding, E. J. Steig, D. S. Battisti, M. Küttel, *Nat. Geosci.* **4**, 398–403 (2011).
29. X. Li, D. M. Holland, E. P. Gerber, C. Yoo, *Nature* **505**, 538–542 (2014).

ACKNOWLEDGMENTS

This work was supported by European Union (EU) grant 264879 (CARBOCHANGE) (P.L., N.G., D.C.E.B., M.H., S.v.H., and N.M.) and EU grant 283080 (GEO-CARBON) (P.L. and N.G.), both of which received funding from the European Commission's Seventh Framework Programme. F.A.H. was supporteted by ETH research grant CH2-01 11-1. T.T., R.W., and C.S. acknowledge funding for the pCO_2 from ship projects from the Climate Observation Division of NOAA. T.T. and the Ship of Opportunity Observation Program were supported by a grant (NA10OAR4320143) from NOAA. C.S.'s contribution to this research was made possible by support from the U.S. National Science Foundation's Office of Polar Programs (grants AOAS 0944761 and AOAS 0636975). B.T. was funded through the Antarctic Climate and Ecosystems CRC, the Australian Climate Change Science Program, and the Integrated Marine Observing System. N.M. is grateful for support from the Institut National des Sciences de l'Univers/Centre National de la Recherche Scientifique and the Institut Polaire Française for the Océan Indien Service d'Observation cruises. C.R. thanks the providers of atmospheric CO_2 measurements and the Deutsches Klimarechenzentrum computing center for their support. SOCAT is an international effort, supported by the International Ocean Carbon Coordination Project, the Surface Ocean Lower Atmosphere Study, and the Integrated Marine Biogeochemistry and Ecosystem Research program, to deliver a uniformly quality-controlled surface ocean CO_2 database. The many researchers and funding agencies responsible for the collection of data and quality control are thanked for their contributions to SOCAT. We also thank A. Hogg for fruitful discussions. The surface ocean CO_2 observations are available from the SOCAT website (www.socat.info). The sea surface pCO_2 and air-sea CO_2 flux data leading conclusions of this manuscript are available to the public via the Carbon Dioxide Information Analysis Center (http://cdiac.ornl.gov/oceans/SPCO2_1982_2011_ETH_SOM_FFN.html). The mixed-layer scheme and inversion data supporting the main findings can be obtained from www.bgc-jena.mpg.de/~christian.roedenbeck/download-CO2-ocean/ and www.bgc-jena.mpg.de/~christian.roedenbeck/download-CO2/. P.L. and N.G. designed the study and wrote the paper together with F.A.H. P.L. developed the neural network estimation and performed the majority of the analyses, assisted by F.A.H. C.R. developed the mixed-layer scheme and the atmospheric inversion. S.v.H., M.H., N.M., C.S., T.T., B.T., and R.W. were responsible for the collection of the majority of the surface ocean CO_2 data in the Southern Ocean. D.C.E.B. led the SOCAT synthesis effort that underlies this work. All authors discussed the results and implications and commented on the manuscript at all stages.

SUPPLEMENTARY MATERIALS

www.sciencemag.org/content/349/6253/1221/suppl/DC1
Supplementary Text
Figs. S1 to S12
Tables S1 and S2
References

1 April 2015; accepted 30 July 2015
10.1126/science.aab2620

PLANT SCIENCE

Six enzymes from mayapple that complete the biosynthetic pathway to the etoposide aglycone

Warren Lau and Elizabeth S. Sattely*

Podophyllotoxin is the natural product precursor of the chemotherapeutic etoposide, yet only part of its biosynthetic pathway is known. We used transcriptome mining in *Podophyllum hexandrum* (mayapple) to identify biosynthetic genes in the podophyllotoxin pathway. We selected 29 candidate genes to combinatorially express in *Nicotiana benthamiana* (tobacco) and identified six pathway enzymes, including an oxoglutarate-dependent dioxygenase that closes the core cyclohexane ring of the aryltetralin scaffold. By coexpressing 10 genes in tobacco—these 6 plus 4 previously discovered—we reconstitute the pathway to (−)-4′-desmethylepipodophyllotoxin (the etoposide aglycone), a naturally occurring lignan that is the immediate precursor of etoposide and, unlike podophyllotoxin, a potent topoisomerase inhibitor. Our results enable production of the etoposide aglycone in tobacco and circumvent the need for cultivation of mayapple and semisynthetic epimerization and demethylation of podophyllotoxin.

Although numerous clinically used drugs derive from plant natural products, little is known about their biosynthetic genes, which prevents access to engineered hosts for their production (*1*). Very few complete pathways exist, and only three—artemisinic acid (*2*), the benzylisoquinoline alkaloids (*3*, *4*), and the monoterpenoid indole alkaloids (*5*, *6*)—have been transferred to a heterologous host for current or future industrial production. Knowledge of plant pathways is especially stark in comparison with the >700 bacterial and fungal biosynthetic pathways that have been characterized (*7*).

Podophyllotoxin, a lignan from mayapple, is the natural product precursor to the topoisomerase inhibitor etoposide (*8*–*10*), which is used in dozens of chemotherapy regimens for a variety of malignancies. Although etoposide is on the World Health

Department of Chemical Engineering, Stanford University, Stanford, CA 94305, USA.
***Corresponding author. E-mail: sattely@stanford.edu**

The reinvigoration of the Southern Ocean carbon sink

Peter Landschützer *et al.*

Science **349**, 1221 (2015);
DOI: 10.1126/science.aab2620